Design of high-power ridge waveguide 980-nm pump lasers

Michele Goano, Elena Torasso, Ivo Montrosset, Sergio Pellegrino, M. G. Re, et al.

Michele Goano, Elena Torasso, Ivo Montrosset, Sergio Pellegrino, M. G. Re, D. Reichenbach, "Design of high-power ridge waveguide 980-nm pump lasers," Proc. SPIE 2148, Laser Diode Technology and Applications VI, (1 June 1994); doi: 10.1117/12.176643

SPIE.

Event: OE/LASE '94, 1994, Los Angeles, CA, United States

Design of high power ridge waveguide 980 nm pump lasers

M. Goano, E. Torasso, I. Montrosset
Dipartimento di Elettronica, Politecnico di Torino, Corso Duca degli Abruzzi 24, 10129 Torino
S. Pellegrino, M. Re, D. Reichenbach
Alcatel–Telettra Research Center, via Trento 30, 20059 Vimercate (MI)

ABSTRACT

The design of ridge waveguide semiconductor pump lasers poses particular simulation problems, since an accurate modeling of the electric and thermal effects and of the optical guiding capabilities is needed. We developed a model whose selfconsistent application allows the evaluation of, among the others, the threshold current of the lasing mode and the gain margin of the higher order modes, the *P-I* characteristic, the power coupled in the fiber, and the far field pattern. Particular attention was paid to the experimental verification of the transverse single mode operation region, and its evolution at high injection levels. The appropriate conditions for operation in the 150–200 mW single mode output power range have been found.

1 INTRODUCTION

The InGaAs quantum well (QW) lasers emitting at 980 nm have received a great attention in the last years[1] and have progressed rapidly as pumping sources for Er-doped fiber amplifiers and also for application in optical interconnection networks. Ridge waveguide (RW) Fabry-Perot lasers have been reported with good characteristics such as low threshold current,[2, 3, 4, 5] but the major problem is in high power regime were single transverse mode operation should be guaranteed in order to mantain high coupling efficiency with the fiber.

The design of such devices is not simple at all because a careful modeling of all the relevant parameters is needed; in this paper we present a model were all the effects are introduced and simulated with various degrees of accuracy. Since our goal was the creation of an easy-to-use software tool for the structural design of such devices and for the verification of the experimental results, we considered more important to take into account all the relevant effects, than to model with great care only some of them; this choice allowed to realize a computer code running also on a PC. In particular we considered:

- the lateral current spreading above the active region;
- the carrier diffusion in the active region;
- the carrier leakage effect from the active region;
- the temperature device model;
- the temperature effect on material characteristics and waveguiding;
- the waveguide properties using the effective index (EI) model;
- the transverse mode competition;
- the modal mirror reflectivities;
- the coupling of the laser beam with the fiber.

In the following we describe first how these effects have been represented in our model and then we present some results of the simulations.

0-8194-1443-3/94/$6.00

2 THE ELECTRIC MODEL

The implemented electric model takes into account the lateral current spreading in the resistive layers above the active region, the carrier diffusion and recombination in the active region, and the current leakage from the active region.

The results for two analytic models proposed in the literature to take into account the spreading in stripe lasers have been considered[6, 7]; in our case the electrode to active layer distance is reduced to the height from the active layer and the ridge bottom. In Fig. 1 (left) an example of the current injection distribution in the active layer obtained with the two considered method is shown.

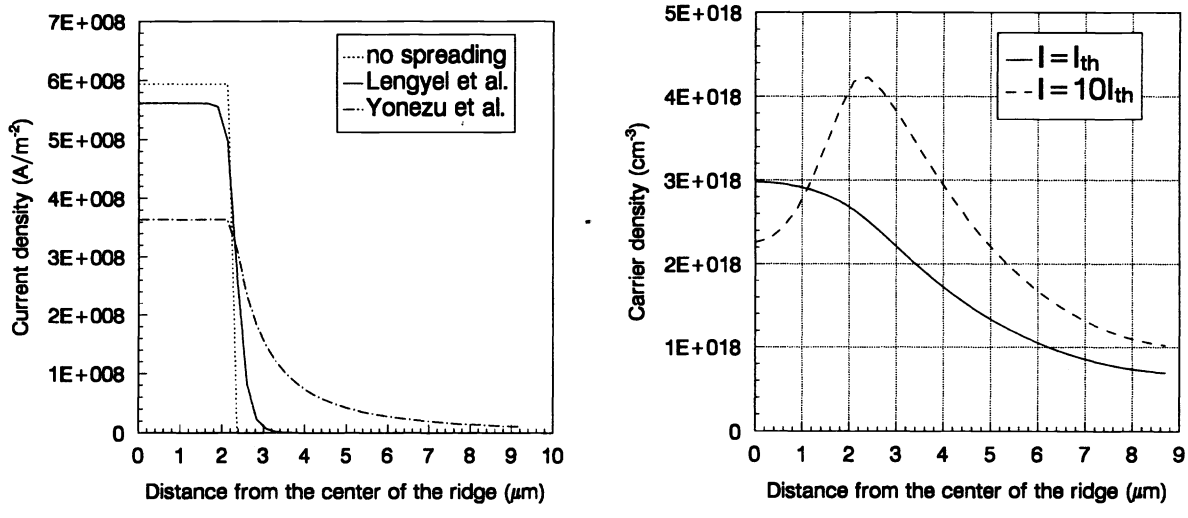

Figure 1: Junction current density obtained using different spreading models (left); carrier density profile at and far above threshold (right). In both cases the ridge width is $2\,\mu$m.

The carrier density profile $N(y)$ is obtained by solving numerically the diffusion equation:[8]

$$D_{\text{eff}}(T)\frac{\partial^2}{\partial x^2}N(y) - R(N(y),T) = \frac{J(y)}{qt} + v_g g_{\text{mat}}(N,T)P$$

where the term depending on the photon density P can be neglected in the small-signal operation or for below-threshold analysis. The carrier recombination has been approximated as:

$$R = AN + B(T)N^2 + C(T)N^3$$

An example of carrier distribution at threshold and far above threshold is shown in Fig. 1 (right), where the effect of the spatial hole burning is quite clearly shown.

A simple analytical model for the electron current leakage across the heterojunction interface has been also implemented. It takes into account only the electrons and holes able to pass the barrier between the active region and the guiding layers.

3 THE THERMAL MODEL

The simple traditional model based on a constant thermal resistance:[9]

$$\Delta T = R_{\text{th}}P_{\text{th}} = R_{\text{th}}(R_s I^2 + V_j I_j - P_{\text{out}})$$

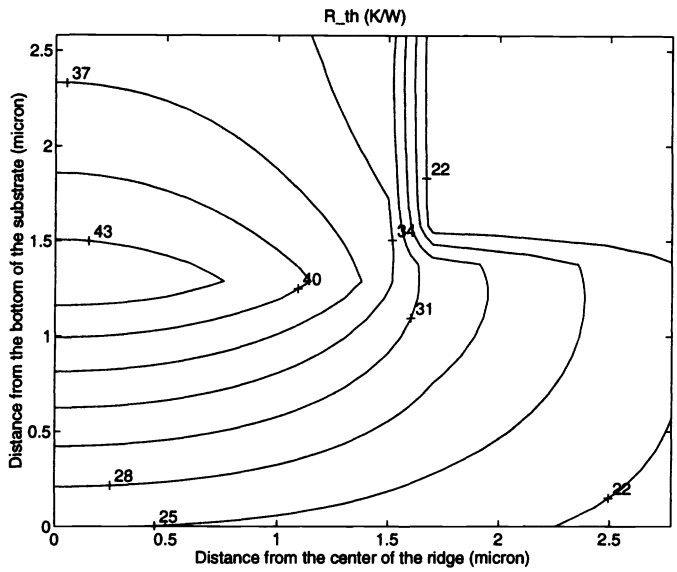

Figure 2: Typical R_{th} map.

where P_{th} is the thermal generated power, V_j is the junction voltage, and I_j is the part of the injected current which contributes to the heat generation in the active region,[9] has been modified to take into account the transverse distribution of the heat generated by the carrier recombination in the active layer. Therefore the contributions of Joule effect and recombination have been associated to different thermal resistances:

$$\Delta T = R_{\text{th,Joule}}\, R_s I^2 + R_{\text{th,ricom}}(x,y)\, (V_j I_j - P_{\text{out}}).$$

and $R_{\text{th,ricom}}(x,y)$ has been obtained by solving the heat flux equation with a finite difference scheme.[10]

In Fig. 2 a map of the temperature for an actual device is shown; the corresponding thermal resistance profiles along the junction and in the orthogonal direction are shown in Fig. 3. Since the optical field is well confined around the active layer and R_{th} is an almost linear function of x, to save memory only the junction temperature profile and the temperature derivatives perpendicular to the junction have been used in our simulator. For a defined structure the previous data have been computed apart, and during the above threshold simulation we supposed that the temperature distribution remains unchanged in the form but is changing its maximum value according to the temperature variation in the center of the ridge.

Beside the influence of the temperature on the local active layer parameter characteristics (material gain, recombination and diffusion coefficients), we considered also the effect on the "bulk" refractive index distribution throught the simple expression:[11]

$$\left.\frac{\partial \ln \varepsilon}{\partial T}\right|_{T_0=300\,\text{K}} = 11.4 \cdot 10^{-5}\,\text{K}^{-1}$$

This change affects the field confinement, and has been verified experimentally.

4 THE ELECTROMAGNETIC MODEL

The modal analysis has been carried out using the effective index method. Since the refractive index variation is much smaller and slower in the transversal y direction we can factorize the electromagnetic problem in depth and transversal directions. Taking y as a parameter, we solve "for every y" the Helmoltz equation along x:

$$\left[\frac{\partial^2}{\partial x^2} + k_0 n^2(x;y)\right] \varphi_i(x;y) = k_0^2 \bar{n}_i(y) \varphi_i(x;y)$$

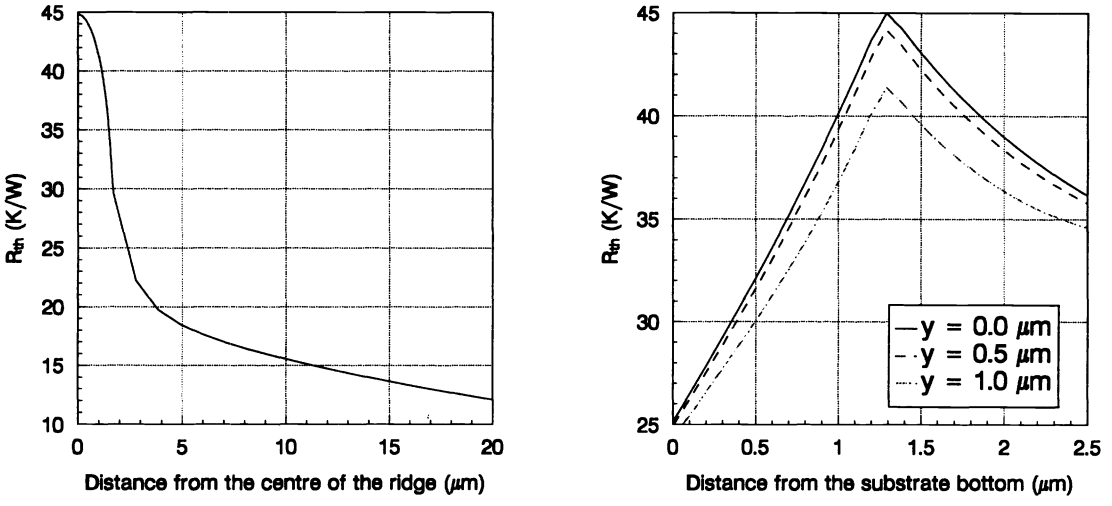

Figure 3: R_{th} behavior along (left) and perpendicular (right) to the junction, corresponding to the map shown in Fig. 2.

We use then the effective refractive index profile $\tilde{n}_i(y)$ as input for the Helmoltz equation along y:

$$\left[\frac{\mathrm{d}^2}{\mathrm{d}y^2} + k_0\tilde{n}_i^2(y)\right]\Phi_i(y) = \beta_i^2\Phi_i(y)$$

Following this procedure we obtain, for given carrier and temperature distributions, the modal gain $g_i = 2\,\mathrm{Im}\{\beta_i\}$, where β_i is the complex propagation constant of the mode, and the modal field distributions $E_y = \Phi_{\mathrm{TE}}(y)\varphi_{TE}(x;y)$ and $H_y = \Phi_{\mathrm{TM}}(y)\varphi_{TM}(x;y)$ for quasi-TE and quasi-TM modes respectively.

In Fig. 4 are reported two examples of effective index and lateral field distribution at and far above the threshold condition. The usual perturbative approach, based on the depth confinement factor Γ_x, which is used to include the effects of $N(y,T)$ on the effective refractive index:

$$\tilde{n}(y) \leftarrow \tilde{n}(y) + \Gamma_x\left[\Delta n(N(y),\lambda) + \mathrm{j}\frac{g_{\mathrm{mat}}(N(y),\lambda)}{2k_0}\right]$$

has been shown inadequate for the high injection operation conditions of power lasers.[12] Therefore we compute $\tilde{n}(y)$ for a large number of values of y having defined:

$$n_{\mathrm{act}} \leftarrow n_{\mathrm{act}} + \Delta n(N(y),\lambda) + \mathrm{j}\frac{g_{\mathrm{mat}}(N(y),\lambda)}{2k_0}$$

where the losses of the passive structure are included in the imaginary part of n_{act}. Simultaneously also the effect of the temperature on each layer has been considered by modifying the refractive indices of the various layers depending on the y and x coordinates.

This procedure introduces only a small penalty in the computation time because the variation of the effective refractive index in adjacent sections is very small and then the convergence of the algorithm is greatly improved.[13] An overall increase of a factor 3 in the computation time has been verified.

5 EVALUATION OF THE FACET REFLECTION AND TRANSMISSION COEFFICIENTS

Dielectric layers are usually applied to the end facets of lasers in order to modify their reflectivity, which is about 0.34 for an uncoated device. The laser light emission is much improved by increasing the reflectivity of the back

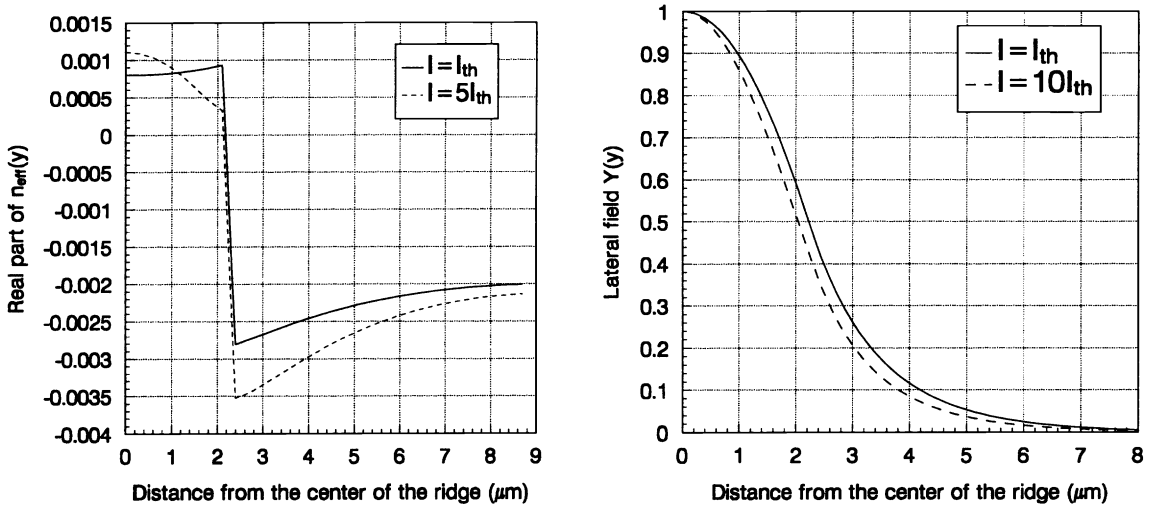

Figure 4: Typical effective index and field profiles at and far above threshold.

facet ($R_{\text{back}} \approx 0.95$ with a multilayer structure) and by reducing the reflectivity of the front facet ($R_{\text{front}} \approx 0.05$: a single layer is enough). Our simulator allows to evaluate these reflectivities from the modal field and refractive index distributions in the waveguide and from the characteristics of the layers deposited on the facets.[14]

In Fig. 5 examples of the wavelength dependence of the reflection coefficient for low (ARC) and high (HRC) reflection coatings are shown.

6 COUPLING OF THE EMITTED LIGHT IN THE OPTICAL FIBRE

ARC and HRC affect significantly the far field pattern; the emitted beam becomes more elliptic, worsening the coupling efficiency with an optical fiber.

The so called correction factor, whose multiplication by the Fourier transform of the field inside the device gives the far field pattern, has been computed with our model for the structures studied by Ohtoshi,[15] and a comparison is shown in Fig. 6. The emitted power coupled in an optical fibre has been computed by means of two methods; one based on a numerical integration of the field overlapping integral and the other on the analytical approximation of the same integral by means of a gaussian interpolation of the transmitted modal field. Fig. 7 shows the comparison between the results obtained by integrating the exact modal field and its gaussian approximation. The excellent agreement allows an immediate extension of this method to the more general coupling problem shown in Fig. 7. In general, the advantage of the use of the gaussian approximation is the practically immediate application to any laser-fiber configuration by means of the matrix formalism for gaussian beam transformation.

7 MATERIAL PARAMETERS

Our simulator needs the knowledge of the following parameters along with their dependence on the alloy composition and the temperature:

- refractive indices (their variation with the temperature can be a relevant effect, since the effective refractive index step is very small);
- effective masses of electrons and holes;
- carrier mobility and ambipolar diffusion coefficient in the active layer;
- resistivity, doping density and optical losses in every layer;

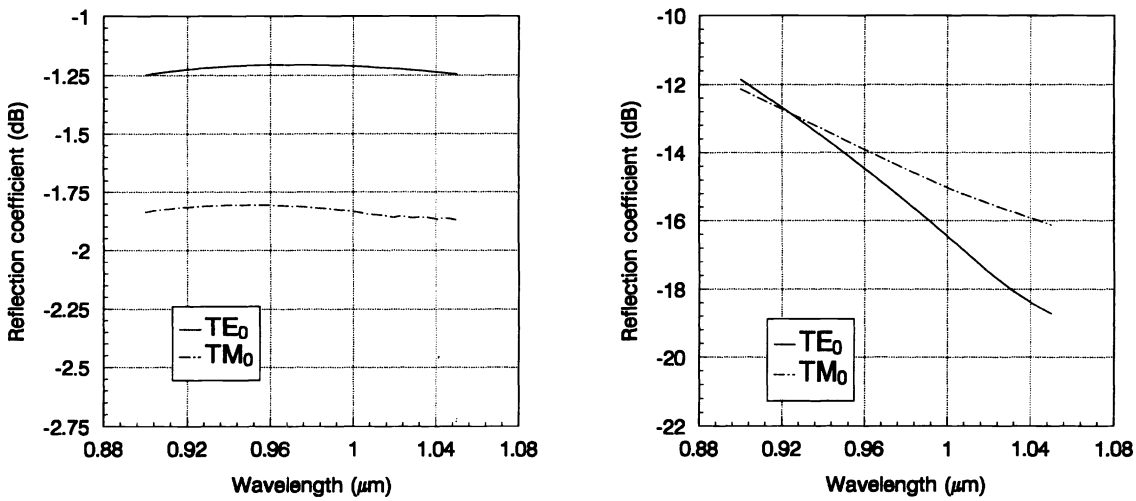

Figure 5: Wavelength dependence of the reflection coefficient (in dB) for a typical HR (left) and AR (right) coating.

- recombination coefficients;
- thermal resistances.

The most important quantities are the optical gain g_{mat} and the carrier induced refractive index change Δn, which can be described with the simple expressions:

$$\begin{aligned} g_{\mathrm{mat}}(N,\lambda) &= a(N-N_0)-\gamma(\lambda-\lambda_p)^2 \\ \Delta n(N,\lambda) &= -\beta N+\delta(\lambda-\lambda_0) \end{aligned}$$

whose parameters can be obtained both from prime-principles calculations and from experiments.

8 THE COMPUTER CODES

Three computer codes have been realized during this activity:

- the first one is mainly devoted to evaluate the modal reflectivities of ARC and HRC. It allows to verify and to correct the typical plane wave approximation design procedure, having the possibility to easily change thicknesses and refractive indices values, and taking into account the effects of current injection;
- the second performs a structural analysis of an active waveguide by evaluating the dependence of the modal parameters from the waveguide structure, the radiation pattern and the fiber coupling with and without AR and HR coatings;
- the third allows a complete analysis of a laser above threshold considering all the relevant effects described in the previous sections.

The second program generates also maps of the modal parameters, allowing the definition of "optimum" waveguides with respect to any prescribed characteristics. For example, it can be used to define optimized structures with respect to modal gain, fiber coupling, etc.

In the third program all the effects presented in the previous sections are solved selfconsistely starting from the structural data of the waveguide and of the coatings, the active layer composition parameters and the thermal resistance map as shown in Fig. 8. The program for this laser structure allows the determination of:

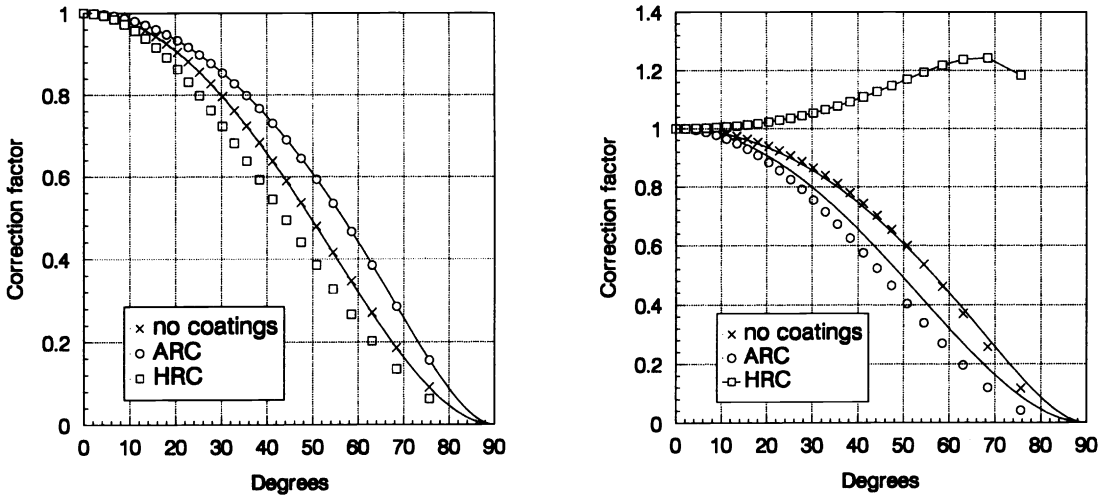

Figure 6: Typical correction factors for the far field perpendicular (left) and parallel (right) to the junction.

- the threshold current of the lasing mode and the gain margin of the higher order modes,
- the *P-I* characteristic and the change in the gain margin of the higher order modes,
- the power coupled in the fiber and the far field pattern,
- the junction voltage vs. injected current characteristic.

9 NUMERICAL RESULTS

In this section we complete the presentation of the numerical results focusing on the features of the simulator. Therefore we are interested in demonstrating the relevance of some physical effects introduced in the model, rather than in the global characteristics of the device.

The device considered is a SQW ridge waveguide laser whose structure is schematically shown in Fig. 9; the most relevant parameters used in the simulation are reported in Tab. 1.

The thermal model has been mainly validated by comparison with experimental results obtained in pulsed regime; in this case the laser temperature can be considered constant and equal to the heat sink temperature. The effect on the threshold current is clearly shown in the right part of Fig. 10.

In the left part of Fig. 10 is reported the threshold current variation with the upper cladding thickness in pulsed and CW regime. The influence of the nonuniform thermal model in the critical region between index-guided and gain-guided regime is shown as an increase of the index guiding region due to the lens focusing effect produced by the heat distribution. During measurement there has been clear evidence of this effect.

In Fig. 11 is shown the gain variation of the lasing mode with respect to high order modes for two different values of the upper cladding thickness. This kind of analysis allows to choose the structure with better single transverse mode characteristic in above threshold operation.

Finally in Fig. 12 the junction voltage vs current characteristic of the laser considered is presented.

All the previously presented results and features of the simulator have been used for the design and the experimental verification of the laser devices manufactured by Alcatel–Telettra. A satisfactory agreement with the experimental results has been eventually obtained.

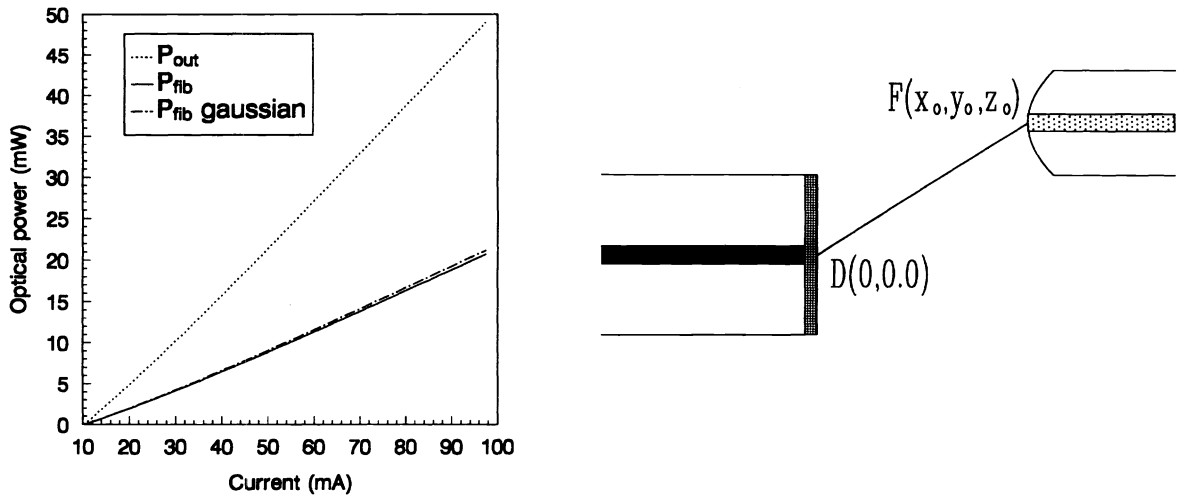

Figure 7: Left: power emitted (dotted line) and coupled into the fiber, estimated using gaussian approximation (dashed-dotted line) and numerical integration (solid line); right: schematic representation of the generic laser-fiber coupling.

CONCLUSIONS

A selfconsistent model for the analysis and structural design of semiconductor ridge waveguide laser has been developed and implemented. Its application to the design of 980nm pump lasers has been presented.

ACKNOWLEDGEMENTS

The autors acknowledge the contribution of Mr. L. Cicchelli in the development of the latest version of the simulator. M.G., E.T. and I.M. acknowledge the partial support from Camera di Commercio di Torino under Research Grant "All-Optical Communication Networks".

REFERENCES

[1] H. Horikawa and A. Ishii, "Semiconductor pump laser technology," *Journal of Lightwave Technology*, vol. LT-11, pp. 167–175, Jan. 1993.

[2] D. P. Bour, N. A. Dinkel, D. B. Gilbert, K. B. Fabian, and M. G. Harvey, "980 nm diode laser for pumping Er^{3+}-doped fiber amplifiers," *IEEE Photonics Technology Letters*, vol. 2, pp. 153–155, Mar. 1990.

[3] M. C. Wu, Y. K. Chen, J. M. Kuo, M. A. Chin, and A. M. Sergent, "High temperature, high power InGaAs/GaAs quantum-well lasers with lattice-matched InGaP cladding layers," *IEEE Photonics Technology Letters*, vol. 4, pp. 676–679, July 1992.

[4] F. Vermaerke, I. Moerman, G. Vermeire, L. Buydens, P. van Daele, and P. Demeester, "Simple reliable processing technique for low-threshold high-power strained InGaAs-AlGaAs GRINSCH SQW laser diodes," *IEE Proceedings-J, Optoelectronics*, vol. 140, pp. 75–79, Feb. 1993.

[5] P. Unger, G.-L. Bona, R. Germann, P. Roentgen, and D. J. Webb, "Low threshold strained GaInP quantum-well ridge lasers with AlGaAs cladding layers," *IEEE Journal of Quantum Electronics*, vol. QE-29, pp. 1880–1884, June 1993.

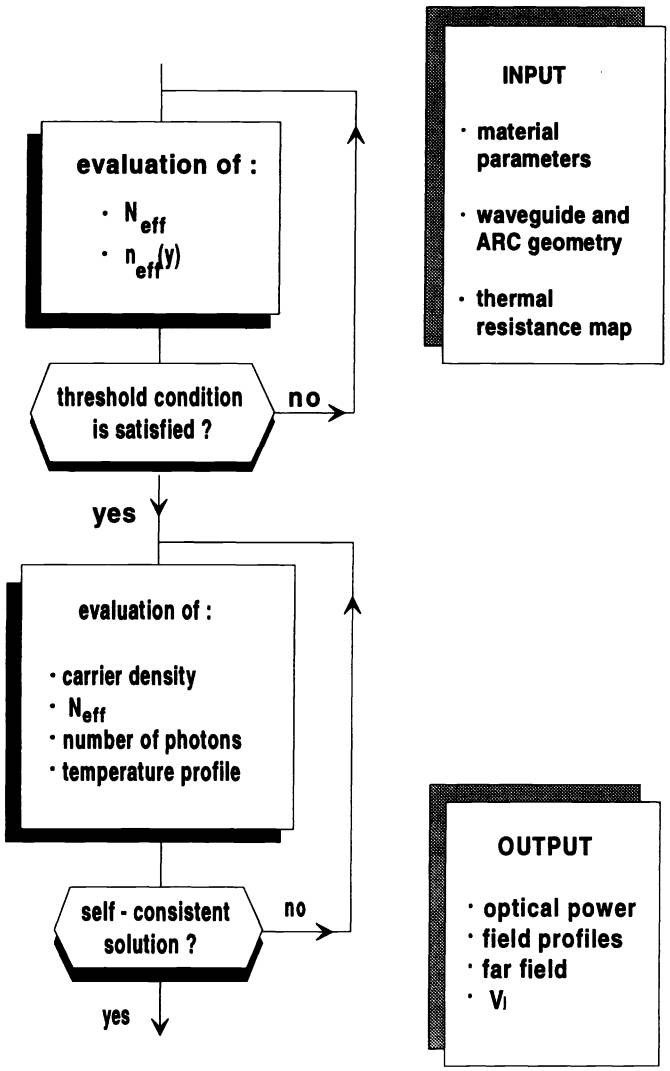

Figure 8: Simplified flow diagram of the laser simulation program

[6] H. Yonezu, I. Sakuma, K. Kobayashi, T. Kamejima, M. Ueno, and Y. Nannichi, "A GaAs-$Al_xGa_{1-x}As$ double-heterostructure planar stripe laser," *Japanese Journal of Applied Physics*, vol. 12, pp. 1585–1592, Oct. 1973.

[7] G. Lengyel, P. Meissner, E. Patzak, and K.-H. Zschauer, "An analytical solution of the lateral current spreading and diffusion problem in narrow oxide stripe (GaAl)As/GaAs DH lasers," *IEEE Journal of Quantum Electronics*, vol. QE-18, pp. 618–625, Apr. 1982.

[8] W. B. Joyce, "Carrier transport in double-heterostructure active layers," *Journal of Applied Physics*, vol. 53, pp. 7235–7239, Nov. 1982.

[9] T. Kobayashi and Y. Furukawa, "Temperature distributions in the GaAs-AlGaAs double-heterostructure laser below and above the threshold current," *Japanese Journal of Applied Physics*, vol. 14, pp. 1981–1986, Dec. 1975.

[10] R. E. Bank, D. J. Rose, and W. Fichtner, "Numerical methods for semiconductor device simulation," *IEEE Transactions on Electron Devices*, vol. ED-30, pp. 1031–1041, Sept. 1983.

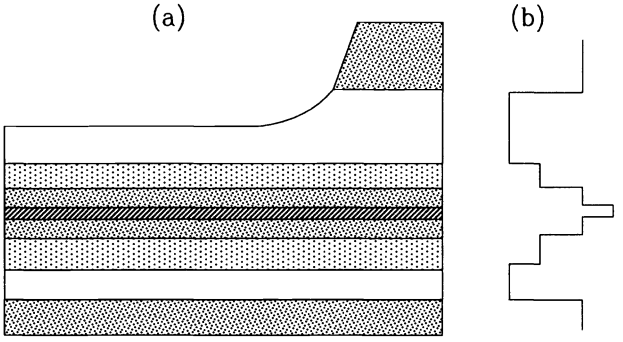

Figure 9: Transverse cross section of a SQW RW laser (a) and corresponding refractive index profile (b).

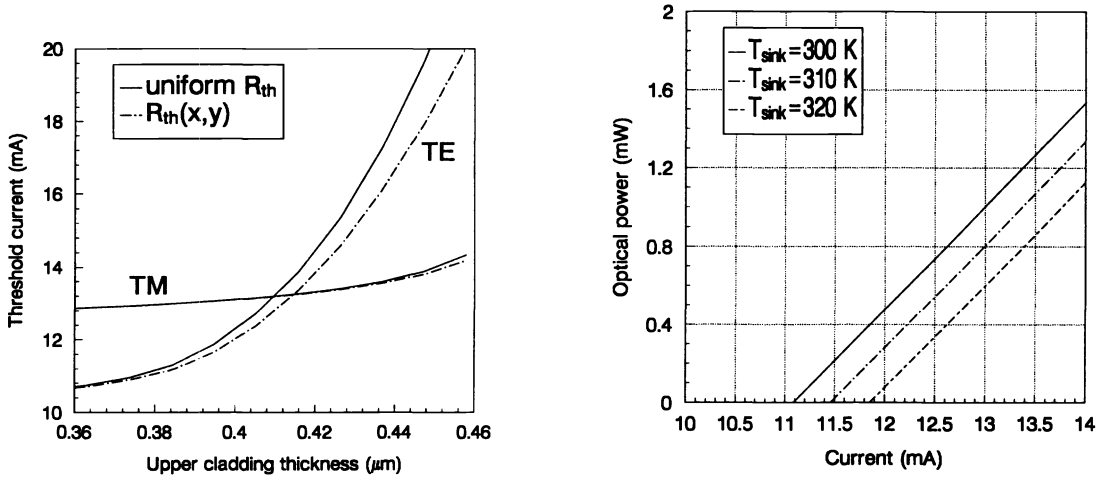

Figure 10: Left: Threshold current of TE and TM fundamental mode as a function of the thickness of the upper cladding d_{up}: pulsed (solid line) and CW (dashed-dotted line) operation. Right: $P(I)$ characteristics in pulsed regime at different heat sink temperatures.

[11] G. A. Samara, "Temperature and pressure dependences of the dielectric constants of semiconductors," in *Gallium Arsenide* (J. S. Blakemore, ed.), vol. 1 of *Key Papers in Physics*, pp. 164–175, New York: American Institute of Physics, 1987. Reprinted from Physical Review B 27, 3494-3505 (1983).

[12] A. P. Bogatov, "Waveguiding and temperature characteristics of threshold current and amplitude-phase coupling coefficient in double-heterostructure lasers," *IEE Proceedings-J, Optoelectronics*, vol. 135, pp. 226–232, June 1988.

[13] M. Goano, I. Maio, and I. Montrosset, "Design of high power low noise polarization insensitive ridge waveguide laser amplifiers," *Journal of Lightwave Technology*, vol. LT-10, pp. 1879–1889, Dec. 1992.

[14] A. G. Failla, G. P. Bava, and I. Montrosset, "Structural design criteria for polarization insensitive semiconductor optical amplifiers," *Journal of Lightwave Technology*, vol. LT-8, pp. 302–308, Mar. 1990.

[15] T. Ohtoshi, "Effect of facet coatings on far fields of semiconductor lasers," *Electronics Letters*, vol. 23, pp. 570–571, May 1987.

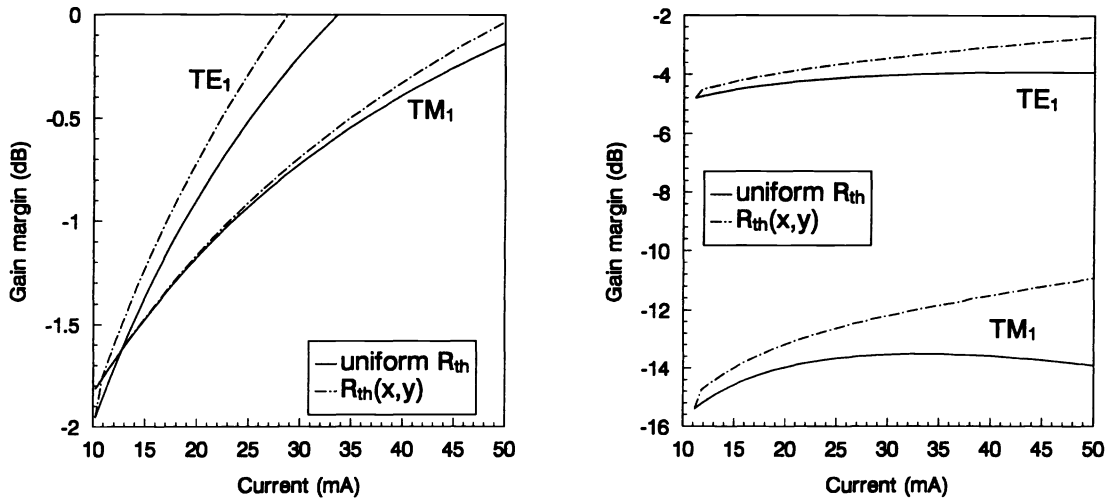

Figure 11: Gain margin of the TE_1 and TM_1 modes as a function of the injected current, for the same structure of Fig. 10. Left: $d_{up} = 0.29\,\mu m$. Right: $d_{up} = 0.38\,\mu m$.

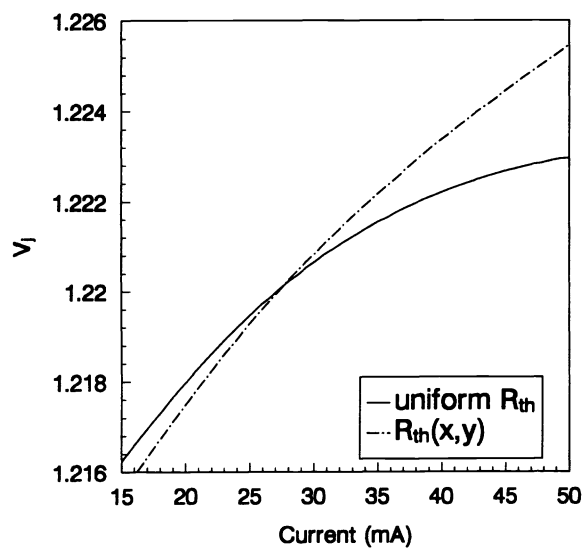

Figure 12: Junction voltage

device length		$500\,\mu m$
recombination coefficients	linear A	$3 \cdot 10^{8}\,cm^{-1}$
	spontaneous B	$1 \cdot 10^{-10}\,cm^{3}/s$
	Auger C	$1 \cdot 10^{-32}\,cm^{6}/s$
gain coefficients	a	$6.3 \cdot 10^{-17}\,cm^{2}$
	N_0	$7.5 \cdot 10^{17}\,cm^{-3}$
resistive layer characteristics	p doping	$2 \cdot 10^{17}\,cm^{-3}$
	Hall mobility	$128.3\,cm^{2}V^{-1}s^{-1}$
other parameters	D_{eff}	$15\,cm^{2}/s$
	group velocity ν_g	$1 \cdot 10^{10}\,cm/s$
	internal losses α_{int}	$6\,cm^{-1}$
	antiguiding β	$-1.8 \cdot 10^{-20}\,cm^{3}$
ridge	composition	$Al_{0.5}Ga_{0.5}As$
	width	$4.5\,\mu m$
	refractive index	3.21
residual lateral cladding	composition	$Al_{0.5}Ga_{0.5}As$
	thickness	$0.291\,\mu m$
	refractive index	3.21
QW active layer	composition	$In_{0.2}Ga_{0.8}As$
	thickness	70 Å
	refractive index	3.55
buffer layers	composition	GaAs
	thickness	60 Å
	refractive index	3.52
cladding layers	composition	$Al_{0.2}Ga_{0.8}As$
	thickness	$0.09\,\mu m$
	refractive index	3.40
substrate	composition	$Al_{0.5}Ga_{0.5}As$
	refractive index	3.21
HRC first layer	composition	Al_2O_3
	thickness	153 nm
	refractive index	1.6
HRC second layer	composition	Si
	thickness	76.5 nm
	refractive index	3.2
ARC	composition	Al_2O_3
	thickness	180 nm
	refractive index	1.6

Table 1: Waveguide and material parameters used in the simulations.